Digest Journal of Nanomaterials and Biostructures

Dig. J. Nanomater. Bios. **2026**; 21(3): 55841
https://doi.org/10.31083/DJNB55841

Original Research

Ni-Doped CoO Nanocomposite Thin Films: Synthesis and Physical Properties

Imad Sharqi[1,*], Rihab Zgueb[1], Hassen Dhaouadi[1], Abdelwaheb Boukhachem[1]

[1]Department of Physics, Faculty of Sciences of Tunis, University of Tunis El Manar, 2092 Tunis, Tunisia
*Correspondence: imadhamoud.ph@gmail.com (Imad Sharqi)
Academic Editor: Carmen-Georgeta Ristoscu
Submitted: 8 November 2025 Revised: 28 March 2026 Accepted: 9 April 2026 Published: 29 July 2026

Abstract

Background: Cobalt oxide (CoO) thin films have attracted considerable interest for sensing and optoelectronic applications owing to their favorable optical and electrical properties. This study investigates the effect of nickel (Ni) doping on the structural, morphological, optical, wettability, and electrical properties of CoO thin films. **Methods:** Pure and Ni-doped CoO thin films (1, 2, and 3 wt% Ni) were prepared by spray pyrolysis and deposited onto glass substrates at 440 °C, resulting in thin films with an average thickness of approximately 200 nm. The films were characterized using X-ray diffraction, morphological analysis, optical measurements, water contact angle analysis, and electrical conductivity measurements. **Results:** X-ray diffraction and morphological analyses revealed irregular structures for both pure and Ni-doped films, with grain size increasing as the Ni content increased. Water contact angle measurements indicated hydrophilic behavior for all films. The optical transmittance reached approximately 85%, while the direct optical band gap varied from 1.98 to 1.90 eV. The extinction coefficient ranged from 0.1 to 3.8 within the wavelength range of 300–1000 nm. Furthermore, the electrical conductivity was strongly influenced by Ni doping. The pure CoO thin films exhibited the highest conductivity, while the Ni-doped films showed lower conductivity values depending on the Ni concentration. **Conclusions:** Ni doping significantly influences the structural, optical, and electrical properties of CoO thin films. The enhanced conductivity, high transparency, and tunable optical band gap demonstrate the potential of Ni-doped CoO thin films for low-cost sensing and practical optoelectronic applications.

Keywords: CoO nanoparticles; X-ray diffraction; energy gap; Ni doping; scanning electron microscopy; electrical properties

1. Introduction

Metal oxides, including copper, zinc, cobalt, and nickel, are potential candidates for a number of significant technical applications, such as solar energy conversion, electronics, magnetic media storage, and catalysis [1]. These oxides have recently formed the basis for the development of nanomaterials for a range of uses. Cobalt oxide nanomaterials are one of these nanomaterials with a variety of shapes and benefits, including low cost, high stability, broadband, and biological compatibility [2]. This material has also been investigated in areas like electrochemical sensors and supercapacitors because of its high selectivity and repeatability [3,4,5]. It is well recognized that the sizes and shapes of the particles play a major role in the behavior of nanophase materials, making them essential components of their functionality and ultimate applications [6]. The regulated size of nanoparticles can provide a variety of electrical, optical, magnetic, and mechanical characteristics in nano-structured semiconductors. Among other uses, porous materials are used as gas sensors and catalysts [7,8]. Nickel and other transition metal oxides with a range of oxidation states are excellent prospects for the next generation's high capacitance. Nickel-based oxides exhibit high specific capacity and promising electrochemical performance, making them attractive materials for energy-storage applications [9]. The creation of cobalt oxide compounds with modifiable physicochemical characteristics has emerged as a field of study, where transition metal doping enhances characteristics such as optical absorption and electrical behavior [10]. In particular, doping cobalt oxide (CoO) with nickel has demonstrated notable alterations in the material's behavior. In addition to the above, nickel-doped Co_3O_4 has been used in previous research and has given effective results in electrochemical performance [11]. Accordingly, we studied the effect of nickel on cobalt oxide. In this work, we investigated the structural, morphological, wettability, optical, and electrical properties of undoped and nickel-doped CoO thin films prepared by spray pyrolysis. The results showed that nickel doping significantly affects all these properties. Most previous studies used nickel concentrations above 3% and did not investigate the changes under lower doping levels. We emphasize that these lower concentrations have not been studied systematically enough, despite their significant impact on some physical properties. We also refer to some studies that used nickel [12,13].

2. Materials and Methods

The temperature at which cobalt oxide thin films were formed was 440 °C in Borj Cedria, Tunisia. CoO acetate dihydrate (Co $(CH_3COO)_2$•$2H_2O$, Merck, Darmstadt, Germany) was used to make the precursor solutions, along with nickel (Ni). First, a 0.1 M solution of cobalt acetate was made by dissolving it in a mixture of deionized water and isopropyl alcohol in a ratio of ¾ to ¼. Acetic acid was added to bring the pH down to 4.7. Ni doping concentrations of 1, 2, and 3 wt.% were achieved by adjusting the precursor composition in the spray solution. After 30 minutes of stirring at room temperature to make sure the resultant solution was clear and uniform, it was sprayed onto a glass substrate at 440 °C. The obtained CoO and Ni-doped CoO thin films had an average thickness of approximately 200 nm.This temperature was chosen in light of earlier spray pyrolysis deposition techniques that proved effective in terms of the quality of thin film preparation. The crystalline properties of both concentrations (Ni) doped with CoO thin films were investigated using an X-ray diffractometer (Phillips (PW3719) X'pert materials research, Philips, Eindhoven, Netherlands) with Cu Kα radiation, scanning from 2θ angles of 10° to 80° at the University of Mosul, Mosul, Iraq. The absorption characteristics of the prepared samples were measured using a Perkin Elmer LAMBDA 1000 UV/Vis/NIR spectrometer (ultraviolet/visible/near-infrared spectroscopy) (PerkinElmer Inc., Waltham, MA, USA) in Baghdad, Iraq. Importantly, all samples were subjected to the same deposition conditions. Then give it enough time to cool the thin films to room temperature. In addition, the samples were subjected to thermal treatment, and the electrical alternating current (AC) conductivity was investigated over the temperature range of 0–225 °C. The samples' wettability was also determined by the water contact angle. Data analysis was performed using OriginPro 2024 software (OriginLab Corporation, Northampton, MA, USA).

3. Results

3.1 XRD Mechanism

Fig. 1 shows the X-ray diffraction (XRD) pattern of pure cobalt oxide thin films doped with nickel at ratios of 1% Ni, 2% Ni, and 3% Ni. The absorption spectrum shows a set of peaks at angles (2θ = 36.5, 42.4, and 61.5°), which are due to cobalt oxide nanoparticles and are consistent with the standard angles for cobalt oxide. It is also worth mentioning that the X-ray spectrum showed the random structure of all the prepared films. As for the rest of the spectra for the nickel doping cases, they included the appearance of two phases that belong to pure cobalt oxide CoO and nickel oxide NiO at angles (2θ = 37.52, 43.16, 62.96, 75.92, and 79.68°). The diffraction angles of cobalt oxide and nickel oxide are very close or may coincide in some cases due to the blue shift or red shift (because of the small difference in lattice parameters (4.261 Å vs 4.177 Å), very slight shifts will appear in the diffraction angles (less than 0.2° at 2θ)). It is also worth noting that the X-ray spectrum showed the random structure of all the prepared films, Fig. 1 [14].

The scientific explanation for the unusual peak, clearly visible in Fig. 1, could be the formation of a secondary phase containing nickel. This would result in a

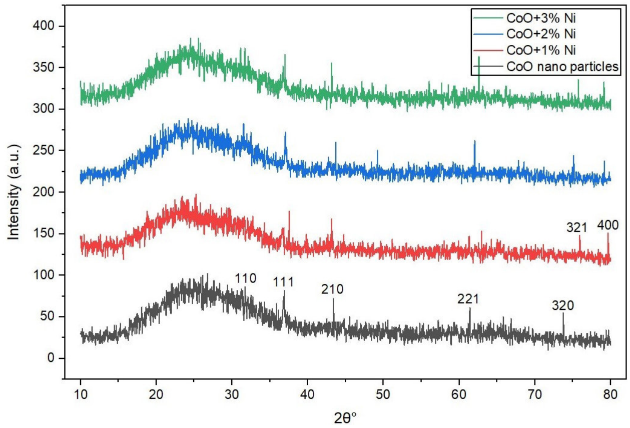

Fig. 1. XRD spectrum of CoO/Ni was deposited at a 440 °C substrate temperature. XRD, X-ray diffraction; CoO, cobalt oxide.

mixed phase such as Co–Ni–O, occurring when Ni is not fully incorporated into the CoO lattice. Alternatively, it could be due to lattice substitution, where the incorporation of Ni^{2+} into Co^{2+} leads to weak additional reflections or peak shifts.

The grain size of all pure doped cobalt oxides was also calculated, and we found that the grain size of pure cobalt was about 57.23 nm. We also found that the dimensions of the nanoparticles increased with the increase in the percentage of nickel, as it was about 47.51 nm for the samples doped with a percentage of 1% Ni, and then the grain dimensions increased to 55.43 nm for the samples doped with a percentage of 3% Ni, as Table 1. These results were consistent with the results of the field emission scanning electron microscopy (FE-SEM) analysis (Fig. 2).

Table 1. XRD results for pure CoO/Ni NPs average grain size (nm).

Materials	Average grain size (nm)
CoO	57.23
CoO + 1% Ni	47.51
CoO + 2% Ni	52.28
CoO + 3% Ni	55.43

NPs, nanoparticles.

The lattice parameter a can be calculated using Bragg's Law [15].

$$2d\sin(\theta) = n\lambda \quad (1)$$

where n is the order of the reflection (n = 1), λ is the wavelength of the X-rays used (1.5406 Å), d is the spacing between crystal planes, and θ is the Bragg angle.

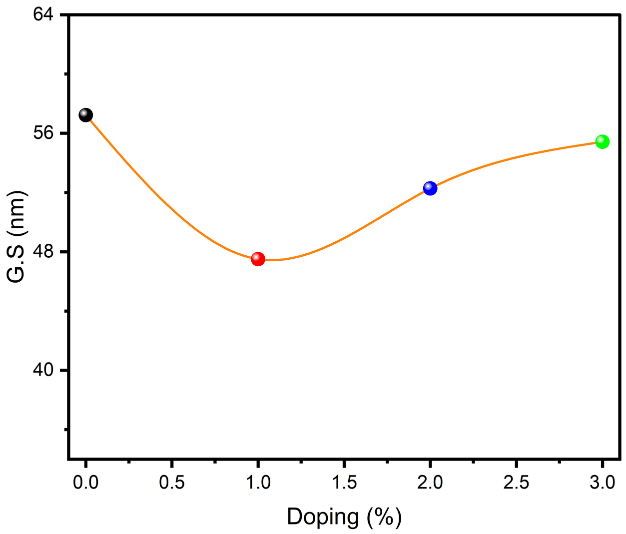

Fig. 2. G.S. as a function of Ni doping ratios for (CoO) films. G.S, grain size.

From the calculation and equation of the cubic system shown below.

$$d = \frac{a}{\sqrt{h^2 + k^2 + l^2}} \quad (2)$$

By substituting Eqn. 2 into Eqn. 1, we obtain the values of the lattice parameter, as shown in Table 2.

Table 2. Estimation of lattice parameter.

Samples	Lattice parameter (Å)
NiO	4.14856
CoO	4.26035

And through the Fig. 3 shows the crystal structure of CoO with the presence of nickel (Ni).

Energy dispersive X-ray spectroscopy (EDX) provides an overview of the sample's composition, including the basic components of the thin film, as well as some elements that appear as a side effect of the chemical reactions involved in preparing the nanoparticles or are added to the sample for the purpose of testing, such as gold [16], which increases the sample's conductivity. Fig. 4 shows the EDX spectrum of the undoped sample, where we notice the presence of only the cobalt element, while the nickel element appears in variable proportions, as we notice an increase in the mass of nickel with an increase in the percentage of nickel doping [17], as shown in Table 3.

3.2 Morphological Mechanism

CoO thin films was imaged by a field emission scanning electron microscope before and after nickel doping (Fig. 5). The grain size of pure and nickel-doped cobalt oxide was calculated. The grain size of pure cobalt oxide was 32.99 nm, while the grain size increased proportionally with increasing nickel doping percentage, from 30.04 nm for 1% doped films to 32.23 nm for 3% doped films (Table 4). In terms of variation in grain size, these results were in good agreement with the XRD spectroscopy (Fig. 6). The CoO-Ni FE-SEM images also revealed the random nature of the prepared films [18,19,20].

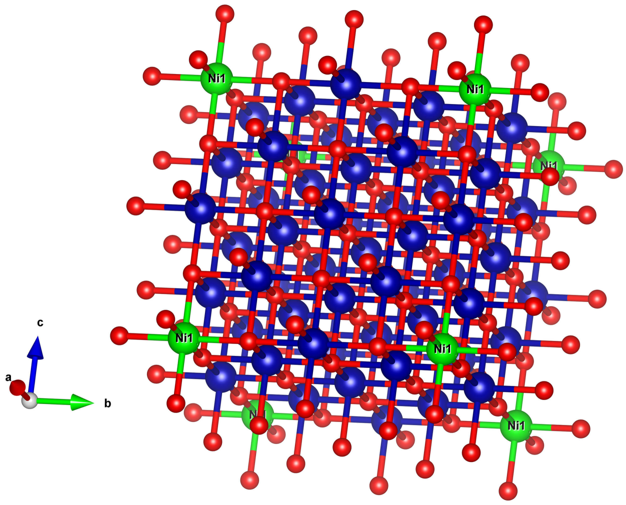

Fig. 3. Crystal structure of CoO/Ni. Ni, nickel.

Table 3. Showing the mass percentage of nickel and cobalt in all samples.

Concentration	Cobalt	Ni
Pure	14.71	0
1%	10.70	0.19
2%	7.87	0.31
3%	13.81	0.33

Table 4. G.S values of CoO thin films prepared by changing the Ni doping ratios.

Materials	Average grain size (nm)
CoO	32.99
CoO + 1% Ni	30.04
CoO + 2% Ni	34.34
CoO + 3% Ni	32.23

3.3 Hydrophilic Phenomenon

The wettability properties of pure and doped cobalt oxide films were studied. As shown in Fig. 7a, the contact angle for all samples was less than 90°, making them hydrophilic. The contact angle depends on the smoothness and roughness of the surface [21,22]. As shown in Fig. 7b, the water contact angles of the thin films prepared on a glass substrate were determined using the fixed droplet method.

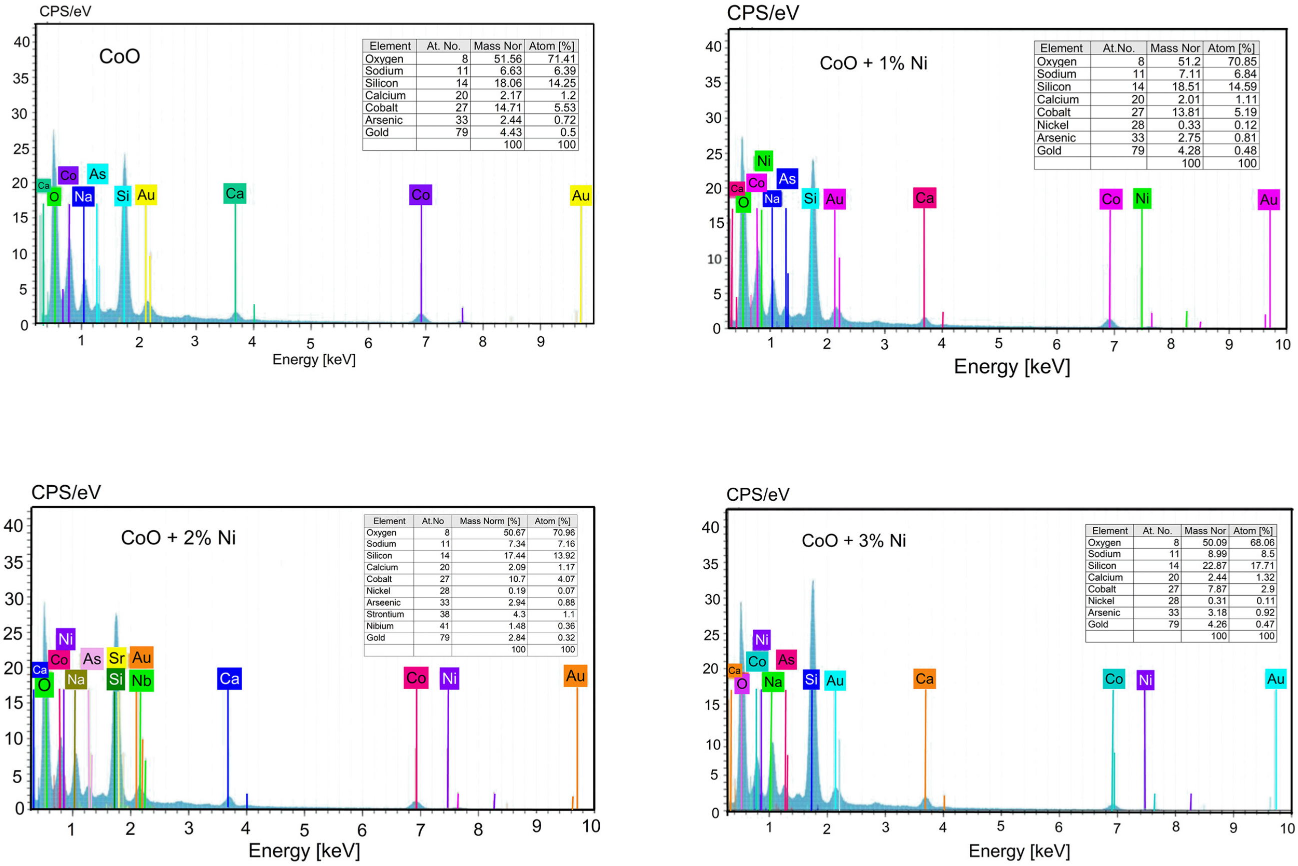

Fig. 4. EDX images of CoO/Ni thin films deposited at 440 °C. EDX, energy dispersive X-ray spectroscopy.

As observed, the pure cobalt oxide thin film exhibited a contact angle of approximately 55.35°. In contrast, the contact angle for the cobalt oxide + 1% nickel samples increased to 59.07°. For the 2% nickel sample, the contact angle was 59.1°. The higher cobalt oxide + 3% Ni films showed an even greater advantage, reaching 59.5°. Thus, the wetting angle can be changed from hydrophilic to hydrophobic by using two substances: ethanol and oleic acid.

3.4 Optical Properties

3.4.1 Fourier Transform Infrared Spectroscopy (FTIR) Mechanism

FTIR measurements were performed on undoped and nickel-doped cobalt oxide thin films prepared at 440 °C with other deposition conditions held constant within a measurement range of 400–4000 cm^{-1}. The peaks at 2833.5 and 2889.5 cm^{-1} in Fig. 8 are organic peaks of organic residues bound to [CH or OH], while the value at 903 cm^{-1} represents the metal oxide peak, specifically cobalt oxide, and may also be for oxides of impure elements. The appearance of the peak at 1134 cm^{-1} indicates an element-oxygen bond, and in the case of doping, it indicates an element-oxygen bond, i.e., the substitution of nickel by cobalt, or the interference of nickel with cobalt in the crystal lattice, forming an element-oxygen-element bond. An increase in the position of this peak indicates better doping. The alignment of the peaks in the region from 500 to 1000 indicates the success of the doping and their alignment in the crystal lattice. This is evident from the shift in the peak at 500, which confirms the peak at 1134 cm^{-1} [23,24].

3.4.2 (R, T) Spectra

Studying the optical properties of thin films is extremely important, as it provides insight into their transmittance and reflectivity properties. For nickel-doped cobalt oxide thin films, we recorded the transmittance (T) and reflectance (R) spectra using a spectrophotometer in the wavelength range of 300 nm to 2000 nm. Fig. 9a,b displays the optical transmission T (λ) and reflection R (λ) spectra for thin films, respectively. It is evident that all transmittance and reflectance spectra lack the interference fringe patterns. In the visible region (400–700 nm), the transmittance varies approximately between 20% and 40%, depending on the Ni content. The transmittance gradually increases at longer wavelengths, reaching higher values in the near-infrared region. The reflectivity does not decrease monotonically with increasing Ni content, indicating a complex dependence on Ni doping level and thin film [23].

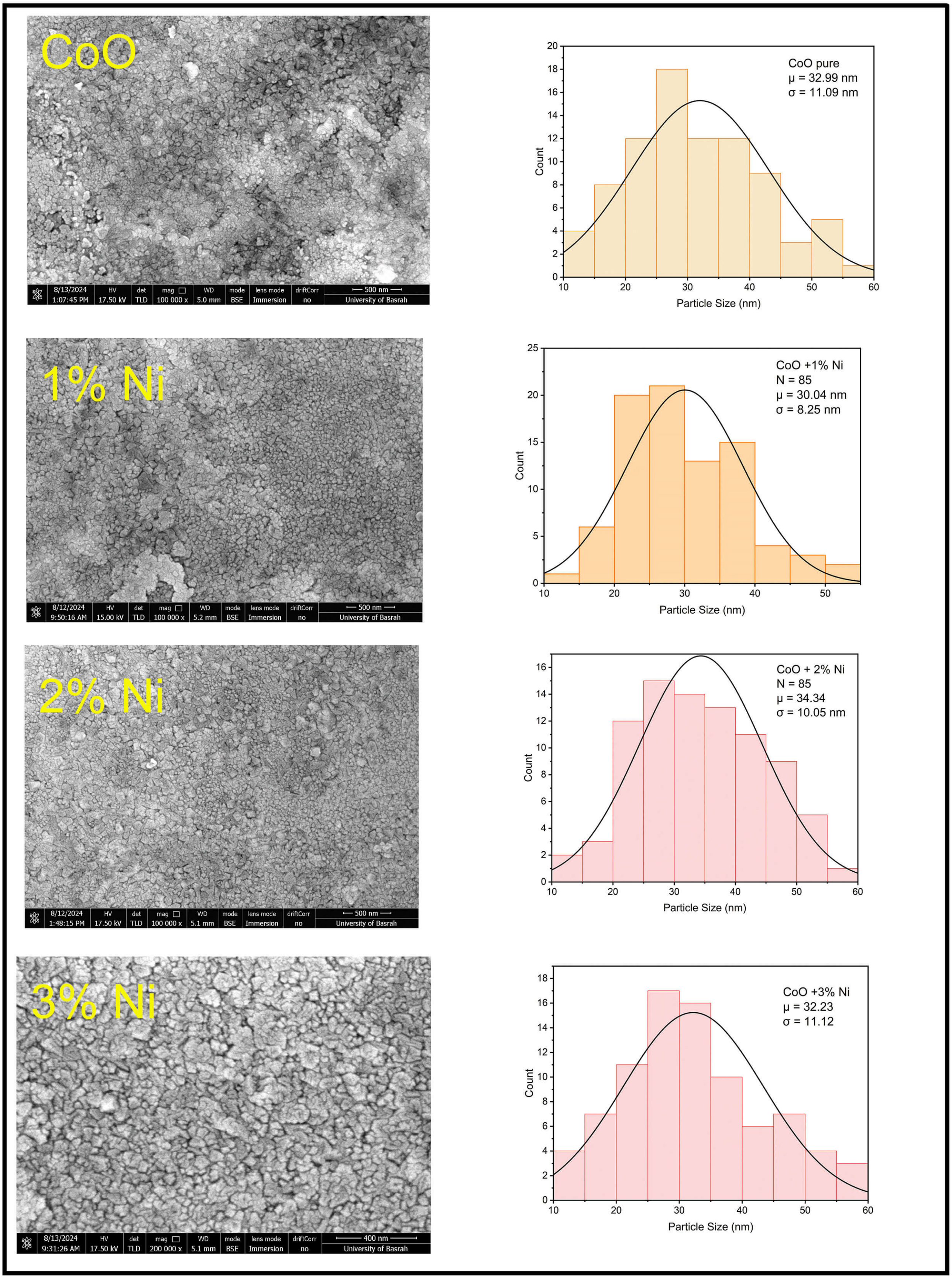

Fig. 5. Shows the FE-SEM images and the distribution of G.S. from CoO/Ni NPs, respectively. Scale bar = 200 nm. FE-SEM, field emission scanning electron microscopy.

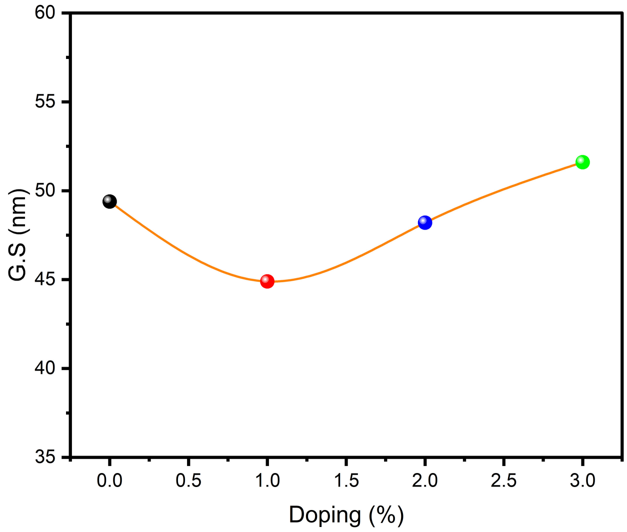

Fig. 6. Grain size as a function of nickel doping ratio for CoO thin films.

3.4.3 Energy Gap

Many factors, including the type of film material prepared and the method of deposition, affect the energy gap. It is also significantly affected by the doping and annealing processes. In addition, the preparation conditions, the nature of the structural composition of the prepared films, and their crystalline regularity affect the energy gap. In general, cobalt oxides exhibit several optical band gaps, which depend on their composition and morphology. Regarding the films studied in this work, the direct energy gap values (Eg) were calculated for pure cobalt oxide films and those doped with nickel at different concentrations. For the optical absorption of CoO/Ni thin films, the conventional relationship in Eqn. 3 was used to analyze the optical absorption data: The direct energy gap is related to the photon energy. The straight line of the curve intersecting the photon energy axis represents the forbidden energy gap value for the allowed direct transition, as shown in Fig. 10. The direct optical band gap values varied between 1.90 and 1.98 eV depending on the Ni concentration. The optical band gap showed a non-monotonic variation with Ni concentration. From this graph, direct optical band gaps of 1.98 eV, 1.90 eV, 1.98 eV, and 1.93 eV were extracted for the cathodes of CoO, 1% Ni, 2% Ni, and 3% Ni, respectively. The extracted band gaps are in good agreement with the reported optical band gap of approximately 2.17 eV for Co_3O_4 [25,26,27,28,29]. Our XRD analysis supports this result.

$$\alpha\, h\upsilon = \mathrm{A}h\upsilon - \mathrm{Eg}^{x} \tag{3}$$

where α is the absorption coefficient α = 1/d ln 1/T, $h\nu$ is the photon energy, E_g the band gap energy and A the edge parameter. The value of x is 2 for indirect allowed transitions and ½ for direct allowed transitions. After doping, direct-gap semiconductor films often exhibit a decrease in the optical band gap energy. In addition, it is known that with increasing doping, the amorphous phase decreases due to more energy being available for crystal formation, which improves the crystallinity of CoO films. Therefore, the band gap reduction of doped CoO films is believed to be due to the increase in crystal size and the decrease in the amorphous phase. The effect of doping on the optical properties of CoO/Ni films is demonstrated by the change in the optical band gap energy [30,31].

3.4.4 UV–Vis Absorption

Absorbance measurements were carried out within the wavelength range of (350 to 1000) nanometers for all undoped and nickel-doped cobalt oxide films with different doping ratios (1%, 2%, 3%). Fig. 11 shows the change in the absorbance spectrum as a function of wavelength, as the absorbance of all films is greatest at short wavelengths. We note that they fall within the visible region and then decrease in a wave-like manner with increasing wavelength. This means physically that the incident photon could not excite the electron and transfer it from the valence band to the conduction band because the energy of the incident photon is less than the energy gap value of the semiconductor, and the absorbance does not show a monotonic decrease with increasing Ni content. The 1% and 2% Ni-doped films exhibit higher absorbance than the undoped CoO film over most of the investigated wavelength range, whereas the 3% Ni-doped film shows relatively lower absorbance values. It is also noted that the absorbance decreases as the percentage of Ni doping with CoO increases compared to undoped films [32].

3.4.5 The Extinction Coefficient

The extinction coefficient represents the amount of attenuation in the intensity of electromagnetic radiation resulting from the interaction of electromagnetic radiation and the particles of the film material, i.e., in other terms, it represents the amount of energy absorbed in the thin film. This parameter, noted as "K" can be calculated using the following relationship (Eqn. 4) :

$$K = \frac{\alpha\lambda}{4\pi} \tag{4}$$

where λ represent wavelength measured in (cm), α absorption coefficient measured (cm^{-1}).

Fig. 12 shows the change in the extinction coefficient as a function of the wavelength of incident photons for pure and Ni-doped cobalt oxide films. The extinction coefficient values ranged from approximately 0.1 to 3.8 over the investigated wavelength range. From the curve, we observe that the extinction coefficient fluctuates with increasing wavelength in the range (300–1000 nm). The extinction coefficient values are high at short wavelengths due to the loss of

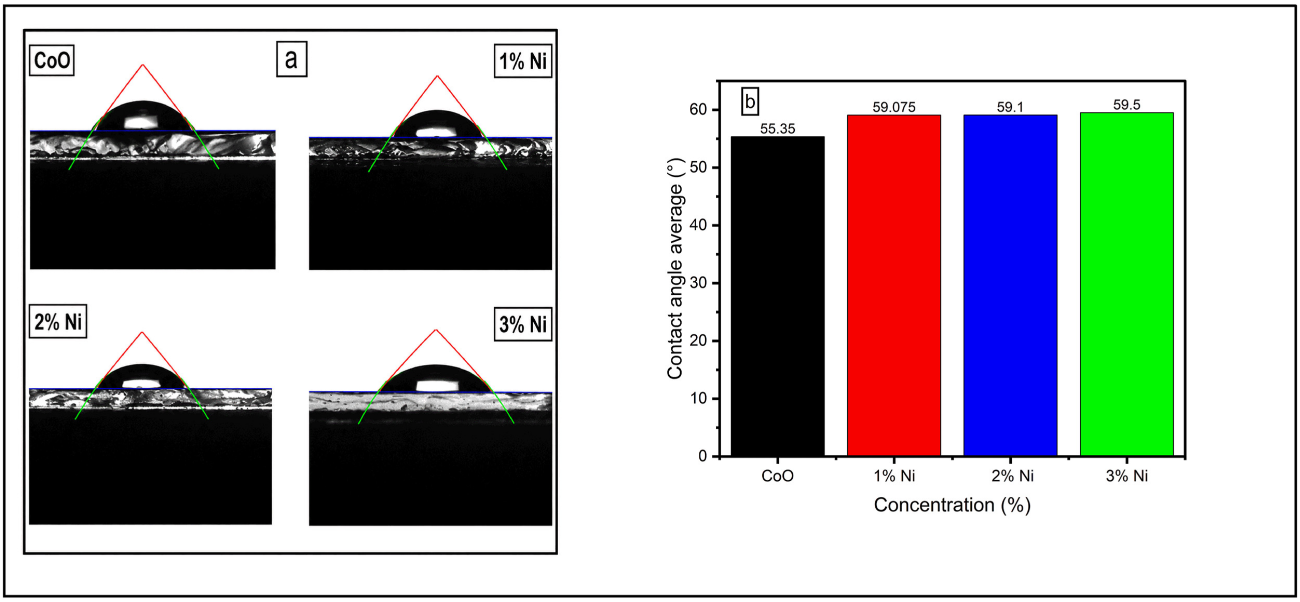

Fig. 7. Hydrophilicity and wettability behavior of CoO thin films as a function of Ni doping concentration. (a) Water contact angle images. (b) Variation of the water contact angle (WCA) with Ni concentration (%).

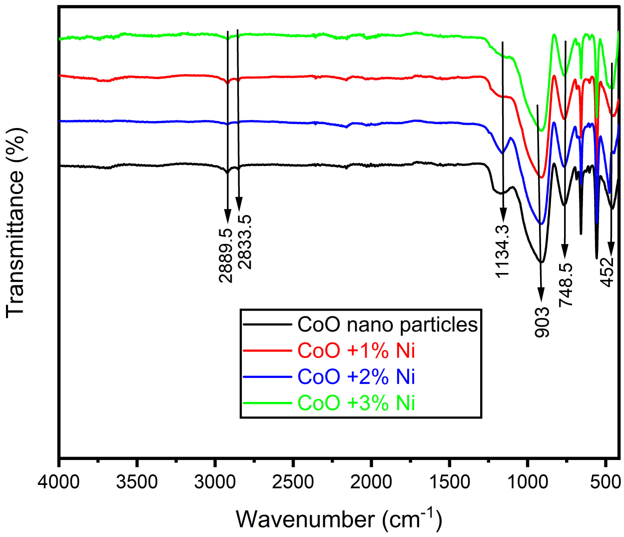

Fig. 8. FTIR spectra of Ni-doped CoO thin films. FTIR, fourier transform infrared spectroscopy.

incident wave energy due to the initial absorption process. The low (K) values at long wavelengths can be attributed to the increased transmittance in that region. The average extinction coefficient values were determined at wavelengths of 550 and 750 nm. The extinction coefficient does not increase monotonically with increasing Ni concentration. The 2% Ni-doped film exhibits the highest extinction coefficient values over most of the investigated wavelength range, while the 1% and 3% Ni-doped films show intermediate values compared with the undoped CoO film. We also observe that the extinction coefficient values fluctuate in all samples. This indicates that the surface of the samples is heterogeneous and suffers from a large absorption of photon energy, which is in complete agreement with the results of X-ray diffraction [14].

3.5 Electrical AC Conductivity Properties

Fig. 13 below shows the changes in electrical AC conductivity values according to different temperature changes for both pure and nickel-doped cobalt oxide. Using mathematical Eqn. 5, the electrical AC conductivity was calculated using the formula:

$$\text{б} = \frac{1}{\rho} \quad (5)$$

where represents AC conductivity, which is the thin film's resistance at a specific temperature. The graph shows that the AC electrical conductivity increases with increasing temperature for all samples. However, the conductivity does not increase monotonically with Ni doping, and the pure CoO thin film exhibits higher conductivity than the Ni-doped films. Since the presence of intrinsic and extrinsic conductors in doped samples increases their excitability with temperature, the AC electrical conductivity of the doped materials increases with increasing temperature. The highest AC electrical conductivity was recorded for the pure CoO sample, reaching approximately 6×10^{-6} S/m at 225 °C [33].

4. Discussion

Nickel incorporation into CoO thin films played an important role in modifying the physical properties of the prepared samples. The observed structural changes after

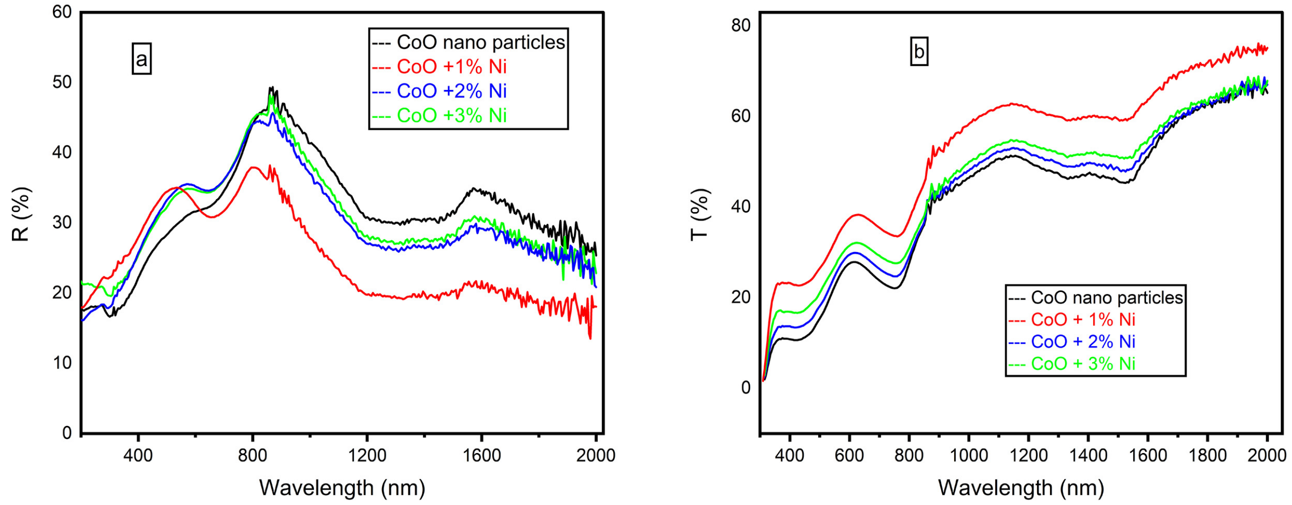

Fig. 9. Optical reflectance and transmittance behavior of pure and Ni-doped CoO thin films over the investigated wavelength range. (a) reflectance (R%) and (b) transmittance (T%).

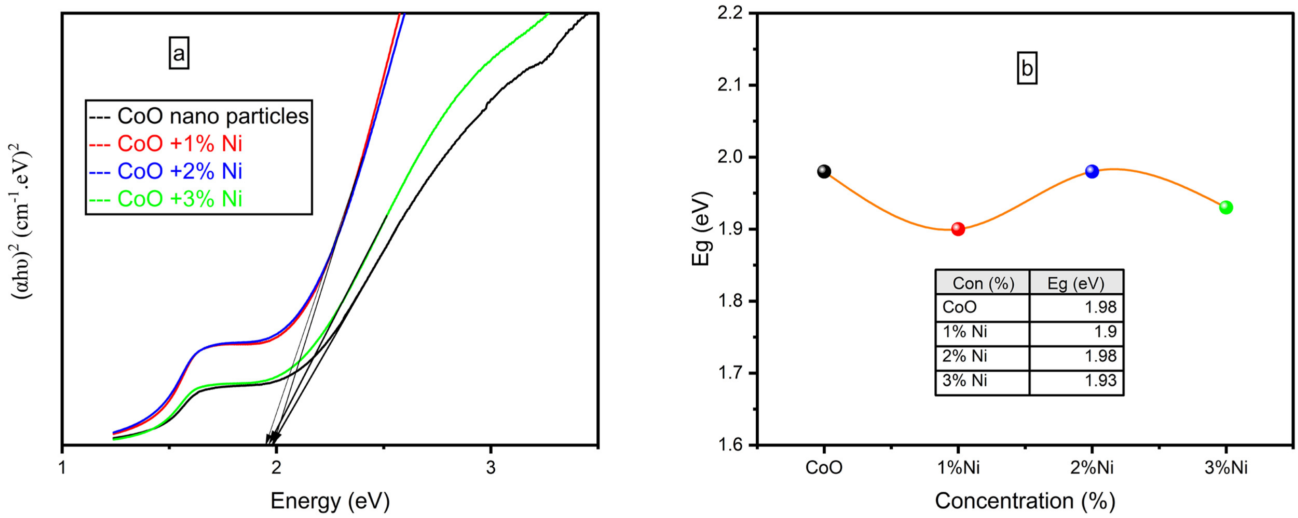

Fig. 10. Optical band gap determination and its dependence on Ni concentration in CoO thin films. (a) Tauc plots of $(\alpha h\nu)^2$ versus photon energy (hν) for pure and Ni-doped CoO samples. (b) Variation of the optical band gap energy (Eg) as a function of Ni concentration (%).

doping suggest that Ni^{2+} ions were successfully incorporated into the CoO lattice, leading to modifications in crystallinity and grain growth behavior. These changes are consistent with previous reports on transition-metal-doped cobalt oxide systems. The reduction in the optical band gap after nickel doping may be associated with the formation of localized energy states and improved crystallinity, which facilitate electronic transitions within the material. In addition, the enhanced optical response and extinction behavior indicate stronger interaction between incident photons and the doped film structure. The gradual increase in contact angle values after doping can be attributed to changes in surface morphology and roughness, which directly influence the wettability behavior of thin films. Although the films remained hydrophilic, nickel doping slightly altered the surface interaction with water droplets. The AC electrical conductivity results indicate that Ni doping does not lead to a monotonic increase in conductivity. The pure CoO film exhibits the highest conductivity, whereas the Ni-doped films show comparatively lower values. This behavior may be related to changes in charge transport pathways, defect distribution, and carrier scattering introduced by Ni incorporation into the CoO lattice. explained by the increased charge carrier concentration and enhanced electron hopping mechanisms inside the CoO matrix. These findings indicate that low-level nickel doping can effectively improve the electrical and optical performance of CoO thin films, which may support their potential use in optoelectronic and sensor applications.

IMR Press

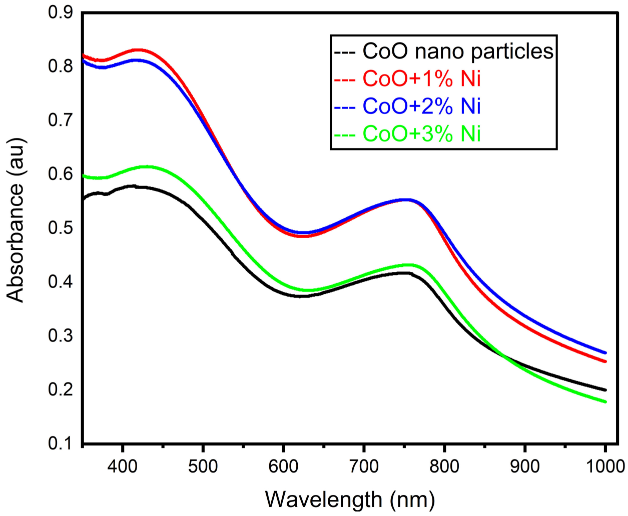

Fig. 11. Absorptivity as a function of wavelength for CoO/Ni thin films.

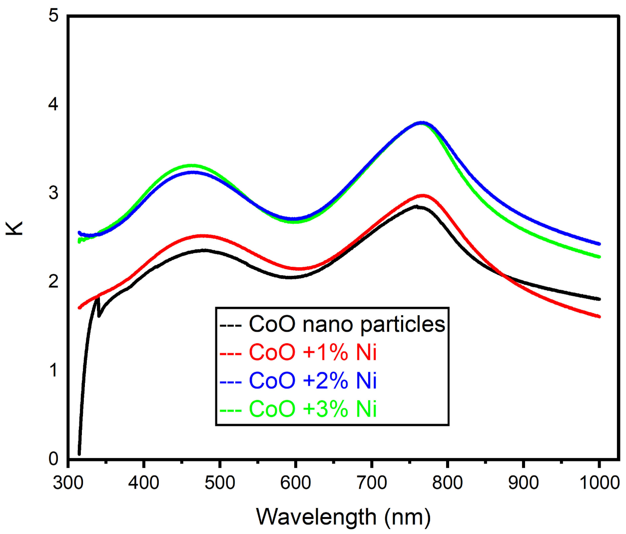

Fig. 12. Plot of K as a function of (λ) for thin film CoO/Ni.

Limitations

This study was limited to low nickel doping concentrations (1–3 wt%) and a single deposition temperature of 440 °C. In addition, long-term stability, magnetic behavior, and advanced electrochemical performance measurements were not investigated. Future studies may focus on wider doping ranges, different preparation conditions, and additional functional characterizations to further optimize the material properties.

5. Conclusions

The structural, morphological, wettability, optical, and electrical properties of undoped and nickel-doped CoO thin films, prepared by spray pyrolysis on glass substrates at 440 °C, were studied. Nickel doping played a significant role in improving the properties. XRD revealed a random structure for both pure and doped cobalt oxide films. The average crystallite sizes of the CoO thin films were found to be between 57.23 and 47.51 nm. FE-SEM revealed the random nature of the pure and doped films. Furthermore, increasing the nickel doping concentration results in finer microstructures and improves the surface density and flatness of the CoO thin films. Regarding the wettability property, it was found that the water contact angle with the film was at the highest concentration of 59.5, which indicates that the film is hydrophilic and provides an idea for future researchers to improve this property by changing the doping element. The optical transmittance was found to be very high, reaching 20% and 40% in the visible region of the spectrum. The band gap energy of the (CoO) films decreased from 1.98 to 1.90 with doped nickel content in the structure, and the absorbance was very high. As for the electrical property, which included electrical conductivity, nickel showed a preference at a concentration of 3% Ni, which explores the role of nickel doping in improving the quality and optical-electrical properties of the films.

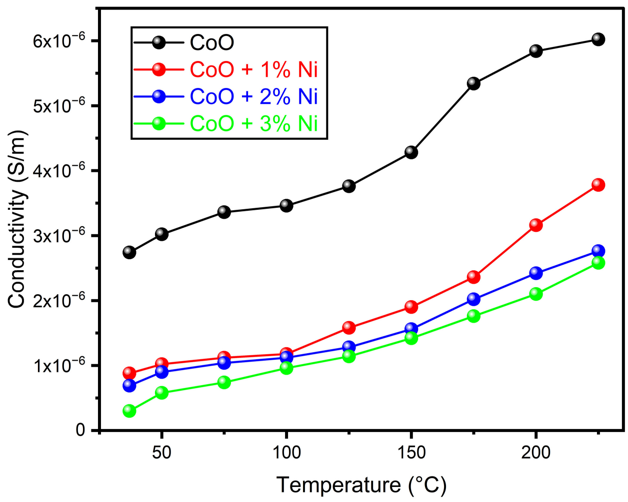

Fig. 13. Electrical AC conductivity of CoO/Ni NPs as a function of different temperatures.

Availability of Data and Materials

The datasets used and analyzed during the current study are available from the corresponding author on reasonable request.

Author Contributions

IS performed most of the experimental work, including X-ray diffraction (XRD) characterization and most of the optical measurements, analyzed the data, and contributed to the interpretation of the results. RZ carried out the electrical conductivity measurements and contributed to data collection. AB prepared the samples and contributed to the experimental procedures. HD designed and supervised the research and prepared the original manuscript draft. All authors contributed to the editorial changes in the manuscript, read and approved the final version, and agreed to be accountable for all aspects of the work.

Ethics Approval and Consent to Participate

Not applicable.

Acknowledgment

Here we would like to express our gratitude to Assistant Professor Dr. Abdul-Khaliq Ayub Al-Rawaji from Iraq, University of Mosul, Department of Physics, Thin Film Specialist, for his valuable scientific guidance.

Funding

This research received no external funding.

Conflicts of Interest

The authors declare no conflicts of interest.

References

[1] Nkele AC, Ezugwu S, Suguyima M, Ezema FI. Structural and electronic properties of metal oxides and their applications in solar cells. In Ezema FI, Lokhande CD, Jose R (eds). Chemically deposited nanocrystalline metal oxide thin films: synthesis, characterizations, and applications (pp. 147–163). Springer: Cham. 2021. https://doi.org/10.1007/978-3-030-68462-4_6

[2] Iravani S, Varma RS. Sustainable synthesis of cobalt and cobalt oxide nanoparticles and their catalytic and biomedical applications. Green Chemistry. 2020; 22: 2643–2661. https://doi.org/10.1039/D0GC00885K

[3] Jang GS, Ameen S, Akhtar MS, Shin HS. Cobalt oxide nanocubes as electrode material for the performance evaluation of electrochemical supercapacitor. Ceramics International. 2018; 44: 588–595. https://doi.org/10.1016/j.ceramint.2017.09.217

[4] Dalkıran B, Kaçar C, Erden PE, Kılıç E. Amperometric xanthine biosensors based on chitosan-Co3O4-multiwall carbon nanotube modified glassy carbon electrode. Sensors and Actuators B: Chemical. 2014; 83–91. https://doi.org/10.1016/j.snb.2014.04.025

[5] Qing X, Liu S, Huang K, Lv K, Yang Y, Lu Z, et al. Facile synthesis of Co3O4 nanoflowers grown on Ni foam with superior electrochemical performance. Electrochimica Acta. 2011; 56: 4985–4991. https://doi.org/10.1016/j.electacta.2011.03.118

[6] Xie X, Ni C, Lin Z, Wu D, Sun X, Zhang Y, et al. Phase and morphology evolution of high dielectric CoO/Co3O4 particles with Co3O4 nanoneedles on surface for excellent microwave absorption application. Chemical Engineering Journal. 2020; 396: 125205. https://doi.org/10.1016/j.cej.2020.125205

[7] Xiao Y, Hu C, Cao M. High lithium storage capacity and rate capability achieved by mesoporous Co3O4 hierarchical nanobundles. Journal of Power Sources. 2014; 247: 49–56. https://doi.org/10.1016/j.jpowsour.2013.08.069

[8] Liang Y, Li Y, Wang H, Zhou J, Wang J, Regier T, et al. Co3O4 nanocrystals on graphene as a synergistic catalyst for oxygen reduction reaction. Nature Materials. 2011; 10: 780–786. https://doi.org/10.1038/nmat3087

[9] Hall DS, Lockwood DJ, Bock C, MacDougall BR. Nickel hydroxides and related materials: a review of their structures, synthesis and properties. Proceedings. Mathematical, physical, and engineering sciences/the Royal Society. 2015; 471: 20140792. https://doi.org/10.1098/rspa.2014.0792

[10] Lakehal A, Bedhiaf B, Bouaza A, Benhebal H, Ammari A, Dalache C. Structural, optical and electrical properties of Ni-doped Co3O4 prepared via Sol-Gel technique. Materials Research. 2018; 21: e20170545. https://doi.org/10.1590/1980-5373-mr-2017-0545

[11] Worku AK, Asfaw A, Ayele DW. Engineering of Co_3O_4 electrode via Ni and Cu-doping for supercapacitor application. Frontiers in Chemistry. 2024; 12: 1357127. https://doi.org/10.3389/fchem.2024.1357127

[12] Ghougali M, Boudine B, Halimi O, Sebais M. Investigation of the physical properties of nanostructured Co:NiO thin films. Chalcogenide Letters. 2021; 18: 765–775. https://doi.org/10.15251/CL.2021.1812.765

[13] Turgut G, Aydın C, Kaya S, Coşkun C. Ultrasonically sprayed cobalt oxide thin films: Enhancing of some physical properties by nickel doping. Materials Letters. 2021; 294: 129962. https://doi.org/10.1016/j.matlet.2021.129962

[14] Kapran A, Hippler R, Wulff H, Olejnicek J, Volfova L, Pisarikova A, et al. Crystalline structure and optical properties of cobalt nickel oxide thin films deposited with a pulsed hollow-cathode discharge in an Ar+O2 gas mixture. Coatings. 2024; 14: 319. https://doi.org/10.3390/coatings14030319

[15] Bragg WH, Bragg WL. The Reflexion of X-rays by Crystals. Proceedings of the Royal Society of London. Series A. 1913; 88: 428–438. https://doi.org/10.1098/rspa.1913.0040

[16] Goldstein JI., Newbury DE, Michael JR, Ritchie NW, Scott JHJ, Joy DC. Scanning Electron Microscopy and X-Ray Microanalysis. 4th Edition. Springer, New York. 2017. https://doi.org/10.1007/978-1-4939-6676-9

[17] Balakrishnan K, Thangavel G, Murugesan N. Structural, morphological, optical and electrochemical aspects of novel synthesized Nickel Oxide and Cobalt doped Nickel Oxide nanoparticles–An alternate electrode material for energy storage devices. International Journal of Nano Dimension. International Journal of Nano Dimension. 2023; 14: 191–202.

[18] Sang Y, Li G, Xue J, Hu J, Tong Y, Liang B, et al. Engineering of metal Co/Ni-CoO nanoparticles embedded in N-doped unclosed hollow carbon nanoboxes as a highly efficient bifunctional electrocatalyst for overall water splitting. Surfaces and Interfaces. 2024; 44: 103729. https://doi.org/10.1016/j.surfin.2023.103729

[19] Ponti A, Ferretti AM, Capetti E, Spadaro MC, Bertoni G, Grillo V, et al. Steering the magnetic properties of Ni/NiO/CoO core-shell nanoparticle films: The role of core-shell interface versus interparticle interactions. Physical Review Materials. 2017; 1: 036001. https://doi.org/10.1103/PhysRevMaterials.1.036001

[20] Lagerqvist U, Svedlindh P, Gunnarsson K, Lu J, Hultman L, Ottosson M, et al. Morphology effects on exchange anisotropy in Co–CoO nanocomposite films. Thin Solid Films. 2015; 576: 11–18. https://doi.org/10.1016/j.tsf.2014.11.064

[21] Li C, Zhang J, Han J, Yao B. A numerical solution to the effects of surface roughness on water-coal contact angle. Scientific Reports. 2021; 11: 459. https://doi.org/10.1038/s41598-020-80729-9

[22] Wang XL, Wang WK, Qu ZG, Ren GF, Wang HC. Surface roughness dominated wettability of carbon fiber in gas diffusion layer materials revealed by molecular dynamics simulations. International Journal of Hydrogen Energy. 2021; 46: 26489–26498. https://doi.org/10.1016/j.ijhydene.2021.05.121

[23] Cardenas FLJ, Chimenos JM, Moreno ALC, Paris EC, Joya MR. Enhancing Co 3 O 4 nanoparticles: Investigating the impact of nickel doping and high-temperature annealing on NiCo 2 O 4/CoO heterostructures. AIMS Materials Science. 2023; 10: 1090–1104. https://doi.org/10.3934/matersci.2023058

[24] Lavanya S, Rajesh Kumar T, Loyola Poul Raj I, Vinoth S, Rimal Isaac RS, Ganesh V, et al. Enhanced structural, optical, and photo sensing properties of Ni-doped Co3O4 thin films prepared by nebulizer spray pyrolysis method. Physica B: Con-

densed Matter. 2023; 649: 414492. https://doi.org/10.1016/j.physb.2022.414492

[25] Dittmer A, da Costa Gouveia TL, Sivalingam K, DeBeer S, Neese F, Maganas D. Revisiting the band gap problem in bulk Co 3 O 4 and its isostructural Zn and Al derivatives through the lens of theoretical spectroscopy. Physical Chemistry Chemical Physics. 2025, 27: 17225–17244. https://doi.org/10.1039/D5CP01735A

[26] Al-Tuwirqi RM, Al-Ghamdi AA, Al-Hazmi F, Alnowaiser F, Al-Ghamdi AA, Abdel Aal N, et al. Synthesis and physical properties of mixed Co3O4/CoO nanorods by microwave hydrothermal technique. Superlattices and Microstructures. 2011; 50: 437–448. https://doi.org/10.1016/j.spmi.2011.06.007

[27] Barakat NAM, Khil MS, Sheikh FA, Kim HY. Synthesis and optical properties of two cobalt oxides (CoO and Co3O4) nanofibers produced by electrospinning process. The Journal of Physical Chemistry C. 2008; 112: 12225–12233. https://doi.org/10.1021/jp8027353

[28] Prieto P, Marco JF, Serrano A, Manso M, de la Figuera J. Highly oriented (111) CoO and Co3O4 thin films grown by ion beam sputtering. Journal of Alloys and Compounds. 2019; 810: 151912. https://doi.org/10.1016/j.jallcom.2019.151912

[29] Louardi A, Rmili A, Chtouki T, Elidrissi B, Erguig H, El Bachiri A, et al. Effect of annealing treatment on Co3O4 thin films properties prepared by spray pyrolysis. Journal of Materials and Environmental Science. 2017; 8: 485–493.

[30] Umeokwonna NS, Ekpunobi AJ, Ekwo PI. Effect of cobalt doping on the optical properties of nickel cobalt oxide nanofilms deposited by electrodeposition method. International Journal of Technical and Applications. 2015; 4: 347–351.

[31] Tharayil NJ, Raveendran R, Vaidyan AV, Chithra PG. Optical, electrical and structural studies of nickel-cobalt oxide nanoparticles. Indian Journal of Engineering and Materials Sciences. 2008; 15: 489–496.

[32] Zribi T, Essaidi H, Bouzourâa MB, Diliberto S, Ottapilakkal V, Touihri S, et al. The effect of tin doping on physical properties of cobalt oxide thin films. Optik. 2023; 293: 171428. https://doi.org/10.1016/j.ijleo.2023.171428

[33] El-Araby M, Mostafa Khalefa M, Mukherjee A, Mohaseb MA, Aboud AA. Physical properties of Ni: Co3O4 thin films and their electrochemical performance. Physica Scripta. 2023; 98: 045816. https://doi.org/10.1088/1402-4896/acc28b